Engineering Metal Adhesion Layers That Do Not Deteriorate Plasmon Resonances

Thomas Siegfried,[†,*] Yasin Ekinci,[†] Olivier J.F. Martin,[‡] and Hans Sigg[†]

[†]Laboratory for Micro- and Nanotechnology, Paul Scherrer Institute, 5232 Villigen-PSI, Switzerland and [‡]Nanophotonics and Metrology Laboratory, EPFL, 1015 Lausanne, Switzerland

ABSTRACT Adhesion layers, required to stabilize metallic nanostructures, dramatically deteriorate the performances of plasmonic sensors, by severely damping the plasmon modes. In this article, we show that these detrimental effects critically depend on the overlap of the electromagnetic near-field of the resonant plasmon mode with the adhesion layer and can be minimized by careful engineering of the latter. We study the dependence of the geometrical parameters such as layer thickness and shape on the near-field of localized plasmon resonances for traditional adhesion layers such as Cr, Ti, and TiO_2. Our experiments and simulations reveal a strong dependence of the damping on the layer thickness, in agreement with the exponential decay of the plasmon near-field. We developed a method to minimize the damping by selective deposition of thin adhesion layers (<1 nm) in a manner that prevents the layer to overlap with the hotspots of the plasmonic structure. Such a designed structure enables the use of standard Cr and Ti adhesion materials to fabricate robust plasmonic sensors without deteriorating their sensitivity.

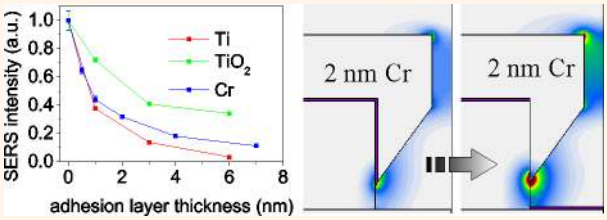

KEYWORDS: adhesion layer · damping · surface-enhanced Raman scattering · near-field simulation · localized plasmon resonance · biosensors

Great amounts of numerical and experimental investigations have been devoted to boosting the signal of plasmonic sensors fabricated from noble metal nanoantennas with sharp edges or with gaps separated by a few nanometers.[1−8] The field enhancement depends mainly on the ability to couple incident photons to localized surface plasmon modes. Such resonant modes are prone to damping by scattering and absorption in the metal and its surrounding materials, thus, limiting the achievable enhancement.[9] By interference with subradiant modes, as in Fano resonant systems, radiative losses can be reduced, but not suppressed completely.[10,11] In any case, the field enhancement is often severely reduced by the presence of adhesion layers. These layers are required to pin the noble metals to the substrate, particularly when the fabrication requires lift-off and sonication or when the applications demand high structural robustness.[12] Thanks to their broad availability and process compatibility with the evaporation of the noble metals, Cr and Ti are the most commonly used adhesion materials, with typical thicknesses ranging between 1 and 10 nm.[13−15] Although the existence of the adhesion layer is an important part of the plasmonic structure, its influence on the near and far field of the plasmonic modes is often neglected.[9,16] The perturbation of the plasmon resonance can be derived from the real and imaginary parts of the adhesion materials dielectric function which affects the refractive index locally and introduces absorption. Under such circumstances, surface and localized surface plasmon resonances (SPR and LSPR) are red-shifted and broadened, leading to reduced signal sensitivities, caused by the reduced quality factor Q of the resonant mode.[17−21] As a consequence, processes where high near-field amplitudes are needed, such as surface enhanced Raman scattering (SERS) and fluorescence,[16,21−23] as well as particle trapping,[24] are weakened.

A route to reduce damping is the use of less absorptive adhesion materials such as Cr_2O_3, TiO_2,[16,25] and ITO,[26] although these

* Address correspondence to thomas.siegfried@psi.ch.

Received for review January 14, 2013 and accepted February 22, 2013.

Published online February 22, 2013
10.1021/nn4002006

© 2013 American Chemical Society

oxides require more specialized preparation and equipment. Another alternative is the use of a self-assembled monolayer such as mercaptosilane, where the silane binds to oxidic surfaces and the thiol end group binds to noble metals.[27] The dielectric environment of the noble metal is found almost unaffected by such a monolayer, and thus, the induced plasmon resonance shift and near-field damping are minimal.[9,21] Unfortunately, the utilization of molecular adhesion layers has severe drawbacks as it requires additional fabrication steps either in wet[21] or dry[9] conditions and the layers may not withstand oxygen plasma or ultraviolet ozone (UVO) cleaning steps indispensible for reusable plasmonic sensors.[12]

In this work, we systematically investigate the damping effect of adhesion layers on the near field enhancement of Au nanostructures. We provide a nanometer precise study of the thickness dependency of metal and metal oxide adhesion layers on the near- and far-field properties of plasmonic nanostructures using SERS and reflection spectroscopy. Additionally, we propose and demonstrate a method to minimize plasmon damping of adhesion layers by excluding the adhesion material from the hotspot (region with the highest near-field enhancement). We further verify for a broad range of Au grating gap sizes and adhesion layer thicknesses that damping is mostly dependent on the overlap between the near-field hotspot and the adhesion layer. Comparison with simulations provides deeper insight into the damping mechanism of adhesion layers and demonstrates how thin adhesion layers can be made without deteriorating their bonding properties. These different strategies enable the realization of plasmonic nanostructures that include metal adhesion layers and do not suffer from damping.

RESULTS AND DISCUSSION

To study the influence of adhesion layers on the performance of plasmonic structures, we utilize periodic nanogap arrays. These were fabricated in a single-step lithography and angular evaporation process. One-dimensional gratings of photoresists with various thicknesses and duty cycles were obtained reproducibly over large areas and with high throughput using extreme ultraviolet interference lithography (EUV-IL).[28] Hydrogen silsesquioxane (HSQ) was used as photoresist, which is converted into SiO_2 upon exposure and development. The adhesion layer and noble metal were evaporated successively onto the photoresist under glancing angles. The substrate was repeatedly tilted to the opposite angle, as shown in Figure 1a, to homogeneously cover the photoresist and controllably reduce the size of the gap.[29] With this technique, we fabricated nanogap patterns with variable thicknesses and gap sizes, with the cross section shown in Figure 1b.

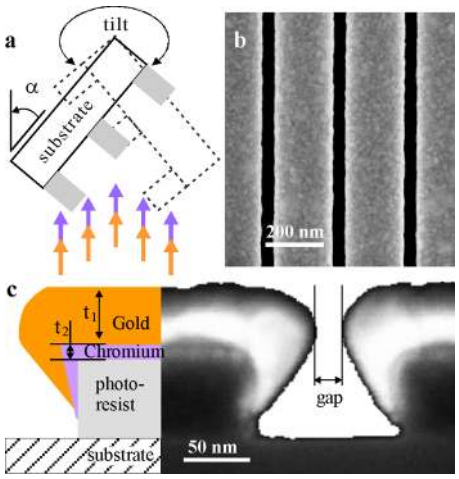

Figure 1. (a) Schematic description of the angular evaporation method, resulting in periodic nanogap arrays. (b) Top view scanning electron micrograph (SEM) and (c) schematic view and SEM of the cross section of the nanogap arrays with the adhesion and gold layers. The pattern is characterized by the gold thickness t_1, the adhesion layer thickness t_2 and the pattern gap size. The cross section is reminiscent of a crescent.

The thus obtained nanostructures consist of an array of crescent shaped line gratings. This configuration, as we will show later, facilitates the generation of strong electromagnetic fields near the crescent tips when the incident light field couples resonantly to the gap-mode of the periodic array.[10] Our nanometer precise and widely adjustable evaporation technique allowed us to study the damping effect of several adhesion layer parameters. The near-field amplitude was quantified using the SERS signal intensity. Thanks to our gentle fabrication process, adhesion layer free patterning was also possible, which we attribute to the clasping of the evaporated gold around the photoresist grating.

The far- and near-field response of our nanogap pattern are simulated for adhesion layers of various thicknesses using a 3D finite element method based on the surface integral solution of Maxwell's equations.[30,31] The far-field spectra in reflection for increasing Cr adhesion layer thicknesses are shown in Figure 2a. The distinctive dip at 680 nm wavelength is attributed to the resonant excitation of the plasmon gap mode, similar to enhanced optical transmission (EOT).[32,33] This resonance exhibits a red-shift with increasing Cr layer thickness, while its amplitude strongly decreases. The second reflection minimum below 500 nm is attributed to the absorbing interband transitions of gold.

At the resonance wavelength of 680 nm, localized plasmons produce a strong near-field at the metal tips of the crescent pattern, as is visible in Figure 2b. The amplitude of this hotspot near the sharp crescent tips significantly decreases for increasing adhesion layer thickness, whereas the near-field in the upper gap region seems not at all affected by the adhesion layer. This suggests that the amplitude of the near-field

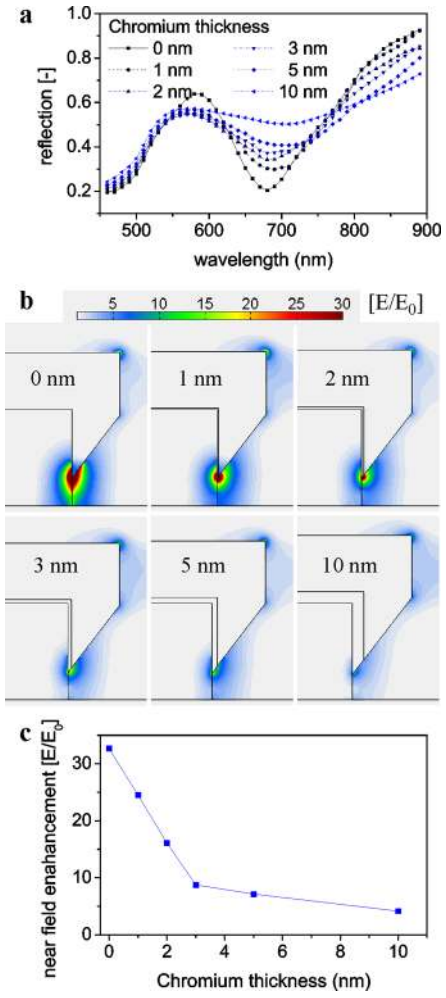

Figure 2. Simulations of the far- and near-field for increasing adhesion layer thicknesses of the crescent pattern with 50 nm Au gap and a period of 250 nm. (a) Far-field reflection spectra, (b) near-field amplitude maps of the crescent array calculated at a wavelength of 680 nm and (c) near-field enhancement, E/E_0, within 5 nm of the crescent tips. The complex refractive indices (n, k) at a wavelength of 680 nm for the 80 nm high photoresist pattern, the Cr with thickness between 0 and 10 nm and the 50 nm Au layer were taken to be (1.39, 0), (3.07, 3.36), and (0.135, 3.88), respectively. The substrate was silicon (3.81, 0.0024). The polarization of the electric field is set across the gaps.

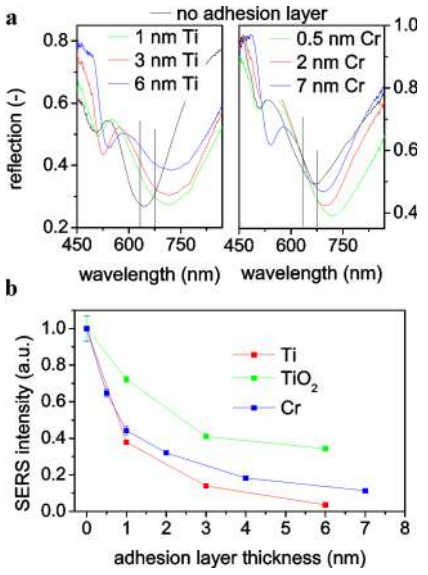

Figure 3. Dependence of the adhesion layer thickness on (a) the reflection spectra for Ti and Cr coatings and (b) the SERS intensity for Ti, TiO_2 and Cr coatings. The laser excitation wavelength at 633 nm and the recorded SERS wavelength at 676 nm, corresponding to a Raman shift of 1008 cm^{-1}, are marked in the reflection spectra. The SERS signal is recorded from a self-assembled benzene−ethane−thiol monolayer deposited on a line array of 50 nm thick Au approximately 40 nm wide gaps. The polarization of the electric field is set across the gaps. Error bars, often smaller than the icon size, represent the standard deviation for 16 spatially separated SERS measurements.

is locally weakened, while the plasmonic mode of the crescent pattern is nearly not altered. We will show that the origin of this phenomenon is the close contact between the electrical field at the hotspot and the adhesion layer. The dependence on the adhesion layer thickness of the damping of the electrical field at the hotspot is shown in Figure 2c. The damping increases strongly with the adhesion layer thickness, resulting in a dramatic loss of the near-field enhancement by a factor of 5 already for a 3 nm thick adhesion layer. This near-field damping on the layer thickness is congruent to what we observe in the SERS measurements, shown below.

The corresponding experiments were performed for adhesion layers made of Cr, Ti and TiO_2. The Au was always evaporated in parallel for each sample series of varying thicknesses, to minimize the influence of metal roughness deviations. Reflection spectra are shown for Ti and Cr in Figure 3a and indicate a 70 nm resonance red-shift, independent of the Ti layer thickness, and a roughly 30 nm red-shift for Cr, slightly changing with the thickness. The resonance broadens and its amplitude decreases with increasing Ti and Cr layer thicknesses, in agreement with the simulation on Cr shown in Figure 2a. The observed blue-shift for increasing the Cr adhesion layer thickness is attributed to an Au gap size reduction of about 5 nm observed when the adhesion layer thickness is increased from 0 to 7 nm. The deviation between Ti and Cr with no adhesion layer could be attributed to a partial liftoff of the Au grating in the Cr sample, caused by weak bonding.

Figure 3b shows the SERS signal intensity dependence on the layer thickness for the three investigated adhesion materials: Ti, TiO_2, and Cr. It is also compared to the near-field decay averaged around the full Au surface. The samples were prepared with a monolayer of benzene−ethane−thiol and were excited and measured at a wavelength of 633 and 676 nm, respectively, corresponding to a Raman shift of 1008 cm^{-1}. We observe indeed a strong reduction of the SERS intensity for adhesion layer thicknesses up to 3 nm. For thicker layers, this damping of SERS levels off,

especially for the Cr adhesion coating. To quantify the strength of the SERS damping, the evolution of the normalized intensity I/I_0 on the adhesion layer thickness is fitted with a power law of the form $(1 + x/nm)^{-a}$, where x is the adhesion layer thickness in nanometers and the exponent a describes the damping rate. An exponent of roughly 0.5 was found for TiO_2, 1 for Cr and roughly 1.5 for Ti. Details of the fitting procedure are given in the Supporting Information, Figure S3. For an adhesion layer thickness of about 6 nm, the SERS intensity was damped by a factor of 2.5 for TiO_2, by 10 for Cr and by 25 for Ti.

As expected, the damping is the smallest for TiO_2, since this material has negligible absorption at this wavelength. The residual damping of a = 0.5 is in part attributed to an incomplete Ti oxidation during evaporation under partial oxygen pressure. The SERS damping is considerably stronger for the metals, because of their large absorption coefficients related to the complex refractive index, $n + ik$. The SERS signal can also decay because of a shift of the resonance, in which case the plasmonic mode is less effectively coupled to the external excitation.[22,34] For Ti and TiO_2, the induced red-shift was around 70 nm, while for Cr, we have observed a red-shift of only 30 nm, shown in Figure 3a and additionally in Figure S1 of the Supporting Information. This may explain the stronger damping of Ti despite its smaller absorption coefficient. In fact, as shown in Figure 3a, the overlap of the excitation and Raman scattering wavelength with the resonance wavelength is best for the sample without an adhesion layer and better for Cr adhesion layers compared to Ti.

The sharp decrease of SERS intensity for adhesion layer thicknesses up to about 3 nm is attributed to the spatial extension of the confined plasmons. The near-field generated by plasmons decays exponentially with the distance from the metal surface and typical decay lengths in metals are in the order of up to 10 nm.[35] Hence, when the adhesion material is located within this plasmon decay length, the damping is strongest. The reduced slope of SERS damping for increasing adhesion layer thicknesses mimics the exponential decay of the plasmon near-field. Conversely, when the adhesion layer remains away from any hotspot, the damping should be minimized, as will be demonstrated below.

Modeling the expected SERS damping with a power scaling of $|E/E_0|^4$, the slope of the experimentally observed SERS damping is found to be smaller compared to the computed decay of the near-field enhancement from Figure 2c. We attribute this behavior to the idealized geometry used in the computation with a point-shaped hotspot, while the real geometry is prone to roughness and corner rounding that spatially expands the hotspot region. In fact, we will demonstrate in the next paragraph that damping is avoided

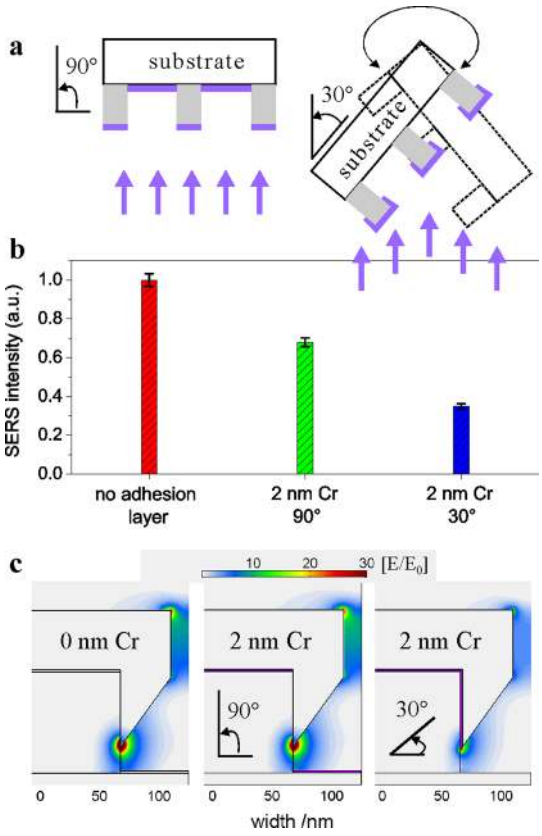

Figure 4. Comparison of SERS signals for vertically and sideward directed Cr layer deposition. (a) Sample orientation for deposition. (b) Observed SERS damping and (c) simulated near-field amplitude maps for a gold crescent array with a 0 nm Cr and 2 nm Cr adhesion layers (drawn in purple) evaporated under 90° and 30° incidence, calculated at a wavelength of 680 nm. The normalized SERS intensities correspond to the 1008 cm^{-1} peak obtained from a self-assembled benzene–ethane–thiol monolayer. The polarization of the electric field as in all other experiments is set across the gaps. Error bars represent the standard deviation for 16 spatially separated SERS measurements. The gold thickness for the periodic pattern was 50 nm and the gap size 30 nm.

when the hotspot is not in direct contact with the adhesion layer.

By changing the evaporation angle for the adhesion material, we could control the contact areas between the adhesion and the Au layers and thus were able to correlate contact area with damping. In the previously discussed experiments, the adhesion material was evaporated at the same angle of 30° at which the shadow evaporation of Au was performed. This enabled the adhesion layer to fully cover the photoresist grating, including the top and the sidewalls. Evaporating the adhesion layer under normal incidence, however, prevents material deposition on the sidewalls of the resist. In a series of experiments with 2 nm thick Cr layers evaporated under 30° and 90°, we observed that the damping of SERS intensity can indeed be strongly reduced by a factor of 2, as shown in Figure 4a.

Since the plasmonic hotspot is located at the crescent tips, as seen in Figure 2b, we attribute the strong

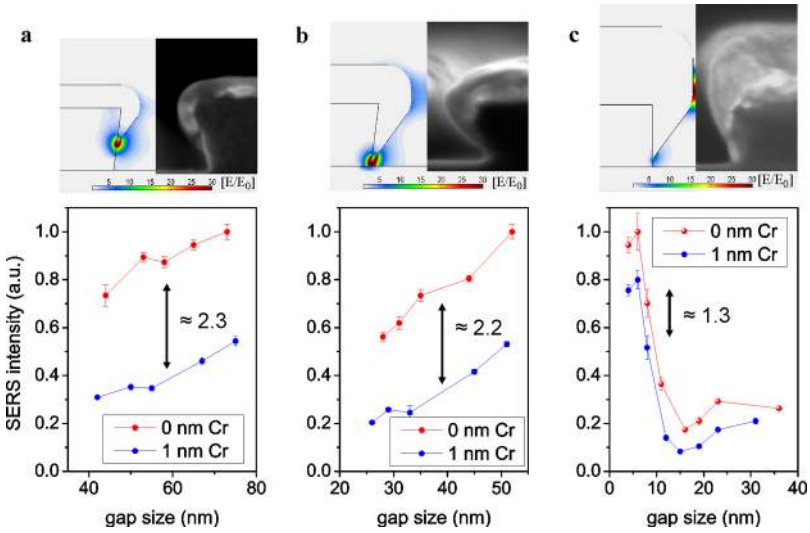

Figure 5. SERS damping for varying gap sizes and metal layer thicknesses of (a) 30 nm, (b) 50 nm, and (c) 80 nm. The Cr was evaporated under ±30° from the surface normal. Near-field amplitude maps are compared with cross section scanning electron micrograph images to relate fabrication parameters to the location of hotspots. The polarization of the electric field is set across the gaps. The normalized SERS intensities correspond to the 1008 cm^{-1} peak of a self-assembled benzene−ethane−thiol monolayer. Error bars represent the standard deviation for 16 individual SERS measurements taken at different locations on the substrate.

SERS improvement to the exclusion of the adhesion material from that tip. Simulations performed in conjunction to the experiments show the strongly reduced field (E/E_0) when the adhesion layer is located at the sidewall of the photoresist (Figure 4c, right panel) compared to the case without contact (Figure 4c, center panel). The near-fields and the plasmon resonances (not shown) for the no- and the distant adhesion layer cases are, however, very similar. Compared to the no-adhesion layer case, the average near-field enhancement (averaged over 5 nm around the hot spot) for the sidewall adhesion layer is about a factor of 3. The SERS damping is less than we would expect from the simple $|E/E_0|^4$ scaling, which we again attribute to the idealized simulation with no roughness and corner rounding. The observed SERS damping, when the adhesion layer is evaporated under 90°, is attributed to an imperfect 90° alignment of the sample during evaporation and the deposition of Cr onto the Si substrate, where it may come into contact with the hotspot, as can be seen from Figure 5b.

The simulations and experiments show that an appropriate adhesion layer design derived from the knowledge of the near-field distribution enables minimizing damping. The finding can also be extended to other nanopatterns requiring lift-off where additional underetching into the adhesion layer and the substrate can reduce the overlap of the adhesion layer with the near-field hot spot, thereby lowering damping.[36]

In our experiments, the durability of the pattern is conserved for both evaporation angles, as long as the adhesion layer remains in contact with portions of the Au interface. This has been verified by treating the different substrates in an ultrasonic bath for several minutes without observing any changes in the SERS intensity. Without an adhesion layer, as shown in Figure 3b, the SERS standard deviation within the tested pattern was observed to be larger than 7%, while it was well below 3% for all the other samples. Intense washing of the substrate and sonication induced a partial lift-off of the Au layer from the photoresist grating when no adhesion layer was used. Remarkably, the pattern did not lift-off for an adhesion layer thickness as thin as 0.5 nm, which was proven by consistent SERS signals for sonication times exceeding 20 min. The same pattern could also withstand several successive cleaning runs without loosing the SERS enhancement.[12] For those experiments, the analyte was removed by 20 min exposure to an Ultraviolet source followed by redeposition of the analyte monolayer. These additional experiments are shown in Figure S2 of the Supporting Information.

We have validated our findings for a broader range of pattern gap sizes and metal Au thicknesses: in all cases, the overlap between the adhesion layer and the plasmons electromagnetic field is found to dominate the damping factor. We have analyzed the damping of SERS intensities for a variety of pattern gap sizes and gold thicknesses. In Figure 5, we compare the SERS signal damping between zero and 1 nm Cr layer for Au thicknesses of 30, 50, and 80 nm and for gap sizes between sub-10 and 75 nm. The gap size of the pattern was set by changing the photoresist duty cycle.

The SERS damping was found to be independent of the nanogap size but depends on the thickness of the Au layer. For Au thicknesses between 30 and 50 nm, the damping is roughly 2.2, while it is 1.3 for 80 nm. This behavior is congruent with simulations showing that

the position of the hotspot does not depend on the gap size but changes its locations from the tip to the nanogap region when the Au thickness becomes larger than about 70 nm, *cf.* comparison between Figure 5a and 5b to 5c. The damping rate of 1.3 is smaller due to the reduced overlap of adhesion layer and hotspot. For the 80 nm thick Au layers and gap sizes below 15 nm, the SERS intensity increases strongly due to stronger coupling between the crescents forming a nanogap channel.[29]

CONCLUSION

We have systematically investigated the geometric constraints associated with adhesion layers such as thickness and overlap with the hotspots and found a route to minimize the near-field damping of localized plasmon resonances. The near-field damping has been quantified by simulations and SERS experiments. The damping has been attributed to the absorption in the adhesion layer, leading to the reduction of the field amplitude, broadening and red shifting up to 70 nm of the resonance wavelength. We find that adhesion layers with a thickness well below 1 nm maintain their adhesive properties, while significantly reducing the damping of the SERS intensity. Outstandingly, the exclusion of the adhesion layer from the proximity of the near-field hotspot reduces damping to a level that was previously only obtained by using metal oxides or monolayers of self-assembled mercaptosilanes. Hence, near-field simulations to locate the hotspots precisely and correspondingly adapted evaporation schemes or underetching of metal adhesion layers into the substrate are the key to realize plasmonic nanostructures with negligible impact on the plasmon resonances. This finding can also be extended to other nanopatterns requiring lift-off, where additional underetching into the adhesion layer and substrate can reduce the overlap of the adhesion layer with the near-field hot spot thereby lowering damping.[36]

To conclude, we could demonstrate that traditional metal adhesion layers with a thickness below 1 nm and deposited with minimal contact to the near-field hotspots produce robust plasmonic nanostructures without deteriorating their performance.

METHODS

Fabrication of Nanogap Arrays. Extreme ultraviolet interference lithography at the Swiss Light Source[28] was used to create line patterns with a period of 250 nm and a height of 80 nm over an area of 1 mm^2 using hydrogen silsesquioxane (HSQ) resist. Glancing angular deposition[37] was used to thermally evaporate the adhesion material and subsequently Au (99.99% purity, purchased from Balzers) layer directly onto the photoresist at a base pressure of 2×10^{-6} mbar. The substrate was aligned at an angle of 30° from the surface plane with an azimuthal orientation of the line pattern perpendicular to the gap expansion (Figure 1a). During evaporation, the substrate was tilted to the mirrored direction (−30°) after every deposited 2 nm, until the final thickness was reached. The adhesion materials Cr and Ti (both 99.99% purity, purchased from Sigma Aldrich) were evaporated at the same angle (30°/−30°) as is the Au or, when specified, evaporation has taken place under normal incidence. TiO_2 was evaporated using the Ti source at a partial oxygen pressure of 5 mbar. The Au was evaporated in parallel for the investigation of sample sequences with varying adhesion layer parameter, to help the accuracy of the evaluation and minimize the influence of metal roughness deviations. The gap size was set by the duty cycle of the photoresist pattern while keeping the evaporated thickness constant. Further details on the fabrication process of the sub-20 nm gap pattern have been reported elsewhere.[29] The adhesion layers were deposited accurately (nm precision of thickness) by placing a quartz balance sensor close to the evaporation source. Thereby, the monitored thickness had to be scaled by 1/3 to factor in the $t \sim x^2$ dependency of the layer thickness t compared to the distance x from the evaporation source.

Optical Measurements. Reflection spectra were recorded with a spatial resolution of about 10 μm using a commercial spectrometer (Sentech FTP) flanged to a microscope (Leica). The incident light was polarized such that the electric field was aligned across the nanogaps. The reflection spectrum obtained from the continuous Au layer on the same substrate served as reference.

The surface-enhanced Raman scattering experiments were performed on a Horiba LabRam HR with a grating resolution of 600 lines mm^{-1}. The excitation source (HeNe laser, 633 nm) with an incident power of 2 mW was focused (50×, numerical aperture NA 0.5) and laterally deflected within an area of 10 × 10 μm^2 of the nanogap pattern to suppress photobleaching. The incident light was linearly polarized with the electric field aligned across the gaps. The average of 16 single spectra was taken over a patterned area of 300 × 300 μm^2 in order to allow for statistical evaluation. The SERS intensities depicted in all figures correspond to the Raman peak of the 1008 cm^{-1} vibrational mode from a self-assembled benzene−ethane−thiol monolayer obtained by 12 h immersion in a 1 mM solution.

Numerical Simulation. The far-field spectra and near-field maps were calculated with a full-field numerical method based on the solution of the surface integral.[30] The simulation of the crescent grating array was carried out in a 3D unit cell with periodic boundary conditions along and across the gap plane. The polarization of the electric field was set across the gap axis. The permittivities for the Si substrate and Cr were approximated with bulk values taken from SOPRA;[38] it is however noted that bulk values can become unreliable for nanometer layer thicknesses. The refractive index of the photoresist HSQ was assumed to be 1.39;[39] the permittivity of Au was taken from Johnson and Christy,[40] and the surrounding medium was air.

Conflict of Interest: The authors declare no competing financial interest.

Acknowledgment. We thank the Swiss National Science Foundation (SNF) for financial support. Part of this work was performed at the Swiss Light Source (SLS), Paul Scherrer Institute, Switzerland.

Supporting Information Available: Cr and TiO_2 reflection spectra; the pattern SERS stability against sonication and UV cleaning; details of the SERS fitting procedure. This material is available free of charge *via* the Internet at http://pubs.acs.org.

REFERENCES AND NOTES

1. Cialla, D.; März, A.; Böhme, R.; Theil, F.; Weber, K.; Schmitt, M.; Popp, J. Surface-Enhanced Raman Spectroscopy (SERS): Progress and Trends. *Anal. Bioanal. Chem.* **2012**, *403*, 27–54.
2. Biagioni, P.; Huang, J.-S.; Hecht, B. Nanoantennas for Visible and Infrared Radiation. *Rep. Prog. Phys.* **2012**, *75*, 024402.

3. Zuloaga, J.; Prodan, E.; Nordlander, P. Quantum Description of the Plasmon Resonances of a Nanoparticle Dimer. *Nano Lett.* **2009**, *9*, 887–891.
4. Duan, H.; Hu, H.; Kumar, K.; Shen, Z.; Yang, J. K. W. Direct and Reliable Patterning of Plasmonic Nanostructures with Sub-10-nm Gaps. *ACS Nano* **2011**, *5*, 7593–7600.
5. Feichtner, T.; Selig, O.; Kiunke, M.; Hecht, B. Evolutionary Optimization of Optical Antennas. *Phys. Rev. Lett.* **2012**, *109*, 127701.
6. Lindquist, N. C.; Nagpal, P.; McPeak, K. M.; Norris, D. J.; Oh, S.-H. Engineering Metallic Nanostructures for Plasmonics and Nanophotonics. *Rep. Prog. Phys.* **2012**, *75*, 036501.
7. Lindquist, N. C.; Nagpal, P.; Lesuffleur, A.; Norris, D. J.; Oh, S.-H. Three-Dimensional Plasmonic Nanofocusing. *Nano Lett.* **2010**, *10*, 1369–1373.
8. Nagpal, P.; Lindquist, N. C.; Oh, S.-H.; Norris, D. J. Ultrasmooth Patterned Metals for Plasmonics and Metamaterials. *Science* **2009**, *325*, 594–597.
9. Habteyes, T. G.; Dhuey, S.; Wood, E.; Gargas, D.; Cabrini, S.; Schuck, P. J.; Alivisatos, A. P.; Leone, S. R. Metallic Adhesion Layer Induced Plasmon Damping and Molecular Linker as a Nondamping Alternative. *ACS Nano* **2012**, *6*, 5702–5709.
10. Gallinet, B.; Siegfried, T.; Sigg, H.; Nordlander, P.; Martin, O. J. F. Plasmonic Radiance: Probing Structure at the Ångström Scale with Visible Light. *Nano Lett.* **2012**, *13*, 497–503.
11. Ye, J.; Wen, F.; Sobhani, H.; Lassiter, J. B.; Dorpe, P. V.; Nordlander, P.; Halas, N. J. Plasmonic Nanoclusters: Near Field Properties of the Fano Resonance Interrogated with SERS. *Nano Lett.* **2012**, *12*, 1660–1667.
12. Siegfried, T.; Kind, M.; Terfort, A.; Martin, O. J. F.; Zharnikov, M.; Ballav, N.; Sigg, H. Reusable Plasmonic Substrates Fabricated by Interference Lithography: a Platform for Systematic Sensing Studies. *J. Raman Spectrosc.* **2012**, *44*, 170–175.
13. Abdelsalam, M.; Bartlett, P. N.; Russell, A. E.; Baumberg, J. J.; Calvo, E. J.; Tognalli, N. G.; Fainstein, A. Quantitative Electrochemical SERS of Flavin at a Structured Silver Surface. *Langmuir* **2008**, *24*, 7018–7023.
14. Fromm, D. P.; Sundaramurthy, A.; Schuck, P. J.; Kino, G.; Moerner, W. E. Gap-Dependent Optical Coupling of Single Bowtie Nanoantennas Resonant in the Visible. *Nano Lett.* **2004**, *4*, 957–961.
15. Cui, B.; Clime, L.; Li, K.; Veres, B. Fabrication of Large Area Nanoprism Arrays and their Application for Surface Enhanced Raman Spectroscopy. *Nanotechnology* **2008**, *19*, 145302.
16. Aouani, H.; Wenger, J.; Gèrard, D.; Rigneault, H.; Devaux, E.; Ebbesen, T. W.; Mahdavi, F.; Xu, T.; Blair, S. Crucial Role of the Adhesion Layer on the Plasmonic Fluorescence Enhancement. *ACS Nano* **2009**, *3*, 2043–2048.
17. Barchiesi, D.; Macías, D.; Belmar-Letellier, L.; van Labeke, D.; Lamy de la Chapelle, M.; Toury, T.; Kremer, E.; Moreau, L.; Grosges, T. Plasmonics: Influence of the Intermediate (or Stick) Layer on the Efficiency of Sensors. *Appl. Phys. B: Lasers Opt.* **2008**, *93*, 177–181.
18. Najiminaini, M.; Vasefi, F.; Kaminska, B.; Carson, J. J. L. Optical Resonance Transmission Properties of Nano-Hole Arrays in a Gold Film: Effect of Adhesion Layer. *Opt. Express* **2011**, *19*, 26186–26197.
19. Sexton, B. A.; Feltis, B. N.; Davis, T. J. Characterisation of Gold Surface Plasmon Resonance Sensor Substrates. *Sens. Actuators, A* **2008**, *141*, 471–475.
20. Lahiri, B.; Dylewicz, R.; De La Rue, R. M.; Johnson, N. P. Impact of Titanium Adhesion Layers on the Response of Arrays of Metallic Split-Ring Resonators (SRRs). *Opt. Express* **2010**, *18*, 11202–11208.
21. Lamy de la Chapelle, M.; Shen, H.; Guillot, N.; Frémaux, B.; Guelorget, B.; Toury, T. New Gold Nanoparticles Adhesion Process Opening the Way of Improved and Highly Sensitive Plasmonics Technologies. *Plasmonics* **2012**, 1–5.
22. Kern, A. M.; Meixner, A. J.; Martin, O. J. F. Molecule-Dependent Plasmonic Enhancement of Fluorescence and Raman Scattering near Realistic Nanostructures. *ACS Nano* **2012**, *6*, 9828–9836.
23. Djaker, N.; Hostein, R.; Devaux, E.; Ebbesen, T. W.; Rigneault, H.; Wenger, J. Surface Enhanced Raman Scattering on a Single Nanometric Aperture. *J. Phys. Chem. C* **2010**, *114*, 16250–16256.
24. Roxworthy, B. J.; Toussaint, K. C. Plasmonic Nanotweezers: Strong Influence of Adhesion Layer and Nanostructure Orientation on Trapping Performance. *Opt. Express* **2012**, *20*, 9591–9603.
25. Jiao, X.; Goeckeritz, J.; Blair, S. Oldham, M., Localization of Near-Field Resonances in Bowtie Antennae: Influence of Adhesion Layers. *Plasmonics* **2009**, *4*, 37–50.
26. Jeppesen, C.; Mortensen, N. A.; Kristensen, A. The Effect of Ti and ITO Adhesion Layers on Gold Split-ring Resonators. *Appl. Phys. Lett.* **2010**, *97*, 263103.
27. Goss, C. A.; Charych, D. H.; Majda, M. Application of (3-Mercaptopropyl)trimethoxysilane as a Molecular Adhesive in the Fabrication of Vapor-Deposited Gold Electrodes on Glass Substrates. *Anal. Chem.* **1991**, *63*, 85–88.
28. Päivänranta, B.; Langner, A.; Kirk, E.; David, C.; Ekinci, Y. Sub-10 nm Patterning using EUV Interference Lithography. *Nanotechnology* **2011**, *22*, 375302.
29. Siegfried, T.; Ekinci, Y.; Solak, H. H.; Martin, O. J. F.; Sigg, H. Fabrication of Sub-10 nm Gap Arrays over Large Areas for Plasmonic Sensors. *Appl. Phys. Lett.* **2011**, *99*, 263302.
30. Gallinet, B.; Kern, A. M.; Martin, O. J. F. Accurate and Versatile Modeling of Electromagnetic Scattering on Periodic Nanostructures with a Surface Integral Approach. *J. Opt. Soc. Am. A* **2010**, *27*, 2261–2271.
31. Gallinet, B.; Martin, O. J. F. Scattering on Plasmonic Nanostructures Arrays Modeled with a Surface Integral Formulation. *Photonics Nanostruct. Fundam. Appl.* **2010**, *8*, 278–284.
32. Ebbesen, T. W.; Lezec, H. J.; Ghaemi, H. F.; Thio, T.; Wolff, P. A. Extraordinary Optical Transmission through Subwavelength Hole Arrays. *Nature* **1998**, *391*, 667–669.
33. Wu, S.; Wang, Q.-j.; Yin, X.-g.; Li, J.-q.; Zhu, D.; Liu, S.-q.; Zhu, Y.-y. Enhanced Optical Transmission: Role of the Localized Surface Plasmon. *Appl. Phys. Lett.* **2008**, *93*, 101113.
34. McFarland, A. D.; Young, M. A.; Dieringer, J. A.; Van Duyne, R. P. Wavelength-Scanned Surface-Enhanced Raman Excitation Spectroscopy. *J. Phys. Chem. B* **2005**, *109*, 11279–11285.
35. Barnes, W. L.; Dereux, A.; Ebbesen, T. W. Surface Plasmon Subwavelength Optics. *Nature* **2003**, *424*, 824–830.
36. Otte, M. A.; Estavez, M. C.; Carrascosa, L. G.; Gonzalez-Guerrero, A. B.; Lechuga, L. M.; Sepalveda, B. Improved Biosensing Capability with Novel Suspended Nanodisks. *J. Phys. Chem. C* **2011**, *115*, 5344–5351.
37. Abelmann, L.; Lodder, C. Oblique Evaporation and Surface Diffusion. *Thin Solid Films* **1997**, *305*, 1–21.
38. Sopra, refraction indices database. www.refractiveindex.info.
39. Yang, C.-C.; Chen, W.-C. The Structures and Properties of Hydrogen Silsesquioxane (HSQ) Films Produced by Thermal Curing. *J. Mater. Chem.* **2002**, *12*, 1138–1141.
40. Johnson, P. B.; Christy, R. W. Optical Constants of the Noble Metals. *Phys. Rev. B* **1972**, *6*, 4370–4379.

Supporting Information to the Manuscript

Engineering Metal Adhesion Layers that Do Not Deteriorate Plasmon Resonances

Thomas Siegfried[†]*, *Yasin Ekinci*[†], *Olivier J.F. Martin*[§], *and Hans Sigg*[†]

[†]Laboratory for Micro- and Nanotechnology, Paul Scherrer Institut, 5232 Villigen-PSI, Switzerland,

[§]Nanophotonics and Metrology Laboratory, EPFL, 1015 Lausanne, Switzerland

AUTHOR EMAIL ADDRESS thomas.siegfried@psi.ch

In analogy with Fig. 3a of the manuscript, the reflection spectra for varying adhesion layer thicknesses are shown in Fig. S1 for other adhesion materials: Cr and TiO_2. The plasmon resonance, seen as a dip around 650 nm, is red-shifted by about 60 nm when introducing TiO_2 adhesion layers and this shift is constant for different layer thicknesses. Note that the small dips around 530 nm are artifacts from referencing the spectra with the reflection from an unpatterned Au area of the same substrate.

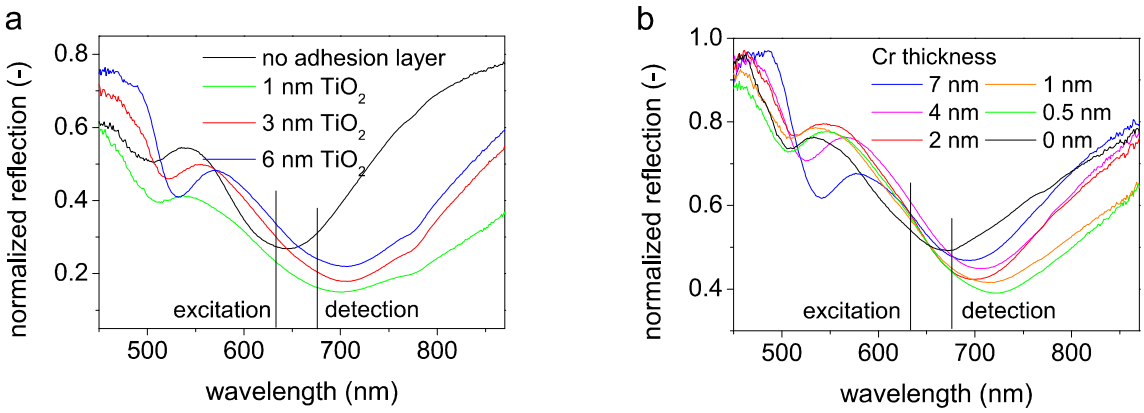

Figure S1. *Reflection spectra for Au nanogap arrays with increasing adhesion layer thickness.* ***a*** *For TiO_2 and* ***b*** *for Cr as adhesion material. The Au thickness of both periodic patterns was 50 nm and the Au gap size was 40 nm. The Raman excitation wavelength at 633 nm and the detection SERS wavelength at 676 nm, corresponding to a wavelength shift of 1008 cm^{-1}, are indicated in the graphs.*

The magnitude of the resonance decreases for increasing adhesion layer thicknesses, similar to Fig. 3a with Ti as adhesion material. When Cr is used as adhesion layer, the red-shift is reduced to about 30 nm together with a reduction of the resonance magnitude for increasing adhesion layer thicknesses. Additionally the resonance position slightly blue-shifts for increasing adhesion layer thicknesses. This blue-shift is attributed to an induced Au gap size reduction of about 5 nm when the adhesion layer thickness is increased from 0 nm to 7 nm.

The pattern stability with a 0.5 nm thick only Cr adhesion layer is shown in Fig. S2. Sonication is applied as well as ultraviolet ozone cleaning to remove the adsorbed molecules at the gold interface.

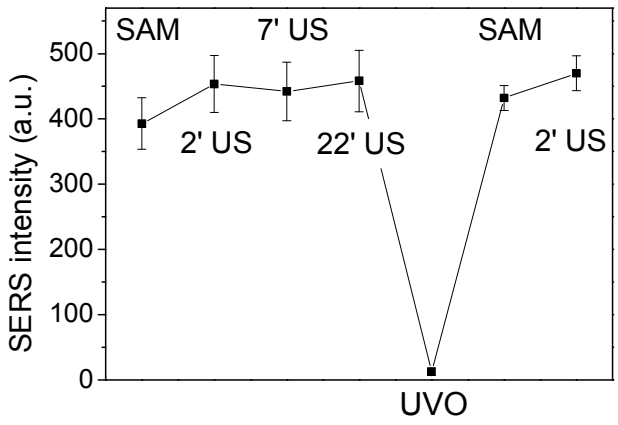

Figure S2. *Pattern stabilized by a 0.5 nm thick Cr adhesion layer evaporated under 90°. The SERS intensity is measured after several exposures to an ethanol ultrasonic bath (US) and for one cycle of cleaning and reforming the benzene-ethane-thiol monolayer. The substrate was cleaned by 20 min ultraviolet ozone exposure (UVO) and repeated rinsing in ethanol. The thiol monolayer was formed during 1 h in a 5 mM benzene-ethane-thiol solution followed by ethanol rinsing (SAM). The Au thickness of the periodic pattern was 50 nm and the Au gap size was 40 nm. The normalized SERS intensities correspond to the 1008 cm^{-1} peak of a self assembled benzene-ethane-thiol monolayer. Error bars represent the standard deviation for 16 spatially separated SERS measurements.*

The SERS intensity was found unchanged after sonication time of for up to 22 minutes. Moreover, the sensor could be cleaned and reused without loosing SERS enhancement. Without the adhesion layer, the Au wire grating partially lifted off from the photoresist pattern and the SERS intensity became strongly irreproducible.

The fitting parameters for the damping rates of varying adhesion layer thicknesses are given in Fig. S3. All SERS measurements were normalized to the SERS intensity at 0 nm adhesion layer thickness. Excellent agreement of the fitted curve with the experimental data was found for Cr and Ti, as well as

for TiO_2.

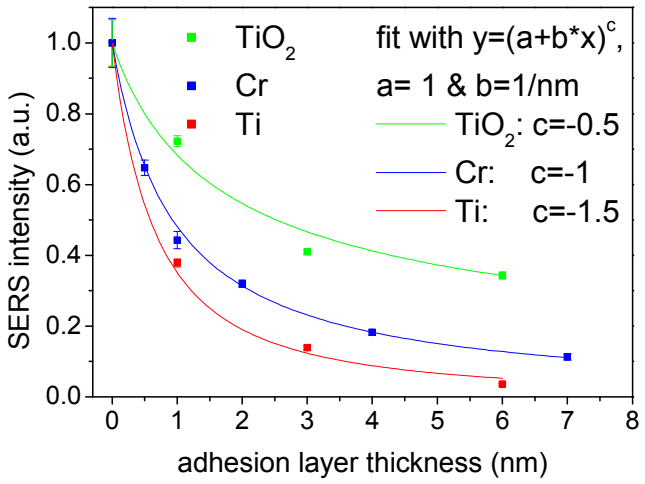

Figure S3. SERS intensity for Titanium, Titanium oxide and Chromium as adhesion material. The experimental data are fitted with the power law dependence $(1+x/\mathrm{nm})^{-a}$, where x is the layer thickness in nm and a the exponent describing the damping. a was fitted with 0.5 for TiO_2, 1 for Cr and 1.5 for Ti. The normalized intensities correspond to the 1008 cm^{-1} Raman peak of a self-assembled benzene-ethane-thiol monolayer. Error bars represent the standard deviation of 16 spatially separated SERS measurements. The gold thickness for the periodic pattern was 50 nm and the gap size was 40 nm.